Influence of Nonuniform Carrier Distribution on the Polarization Dependence of Modal Gain in Multiquantum-Well Lasers and Semiconductor Optical Amplifiers

Dayan Ban and Edward H. Sargent, *Member, IEEE*

***Abstract*—We investigate the modal gain seen by transverse-electric (TE) and transverse-magnetic (TM) modes of bulk and multiquantum-well (MQW) lasers given a nonuniform distribution of active region carriers. We find that the dependence of modal gain on the nonuniformity of carrier profile differs for TE and TM modes. This experimentally observable phenomenon is proposed as a measure of carrier density nonuniformity. We discuss the importance of the confinement picture for TE and TM modes, in the generalized presence of some asymmetry, in assuring injection-level-independent polarization insensitivity in semiconductor lasers and optical amplifiers.**

***Index Terms*—Modal gain, multiple quantum well, nonuniform carrier distribution, semiconductor laser, semiconductor optical amplifier, TE polarization, TM polarization.**

I. Introduction

SEMICONDUCTOR lasers have been known for two decades now to benefit from the use of multiple quantum wells (MQWs). Specific advantages include:

- enhanced differential gain associated with reduced (2-D) density of states, which can in turn be applied to achieving a high modal differential gain and high direct-modulation bandwidth;
- reduced threshold current as a result of suppression of Auger recombination achieved via band-structure engineering;
- higher characteristic temperature.

The advantages and opportunities associated with MQWs are accompanied by challenges. Perhaps of greatest concern is the fact that, in a system with many wells separated by spatially thick or energetically high barriers, injected nonequilibrium carriers may become nonuniformly distributed among the wells [1], [2]. In view of the sublinear relationship between optical gain and carrier density, taken together with the superlinear relationship between nonradiative recombination rates and carrier density, the nonuniform carrier distribution militates against high-performance laser operation. Piprek and coworkers [3] have found that nonuniform carrier distribution in InGaAsP-InP MQW laser diodes causes QW recombination losses to increase with rising injection current above threshold. These losses result in a degradation of the internal differential efficiency. Nonuniform carrier distribution inside the cavity has been proposed to lie at the origin of unusual chirp behavior of a four-electrode bistable distributed Bragg reflector (DBR) laser [4]. In sum, in the presence of a nonuniform distribution of gain-providing carriers, threshold current is increased, external differential efficiency decreases with decreasing stimulated lifetime above threshold, and a degraded modal gain results in worsened dynamic performance.

The subject of nonuniform carrier density distributions has attracted significant attention in the 1990's. Eisenstein and Tessler [5] presented a rate equation model to predict the carrier density distribution among the wells based on carrier capture/escape times. Maciejko *et al.* [6] presented a model which, by accounting for two-dimensional (2-D) carrier injection in a gain-coupled DFB MQW laser with locally etched QWs, showed that hybrid (combined lateral and vertical) injection of holes could be used to lessen interwell nonuniformity and enhance performance.

Li *et al.* employed a spatially- and spectrally-resolved near-field imaging of unstable resonator semiconductor lasers to measure lateral refractive index variation [7]. The technique allowed for the measurement of index changes due to nonuniform carrier distribution, providing a possible indirect route toward the measurement of carrier density nonuniformity. The technique may not be sufficiently sensitive or permit sufficiently high resolution to allow independent measurement of individual QW refractive indices and carrier densities.

While the mechanisms underlying the problem of interwell carrier density nonuniformity have been clarified via numerical modeling, the phenomenon remains to be observed directly via experiment. Whether carrier density nonuniformity among the wells is indeed the chief mechanism responsible for observed performance degradation cannot be resolved conclusively in the absence of experimental measures of the degree of nonuniformity. The resulting lack of confidence as to the key mechanism responsible for performance degradation impedes device performance optimization.

In this paper, we investigate the difference in the dependence of TE versus TM modal gain on the spatial nonuniformity of

Manuscript received January 4, 2000; revised May 17, 2000.

The authors are with the Department of Electrical and Computer Engineering, University of Toronto, Toronto, ON M5S 3G4, Canada.

Publisher Item Identifier S 0018-9197(00)07265-1.

gain-providing carriers. We use simplified analytical calculations and numerical simulations to predict the direct impact of interwell carrier nonuniformity and observable amplified spontaneous emission/gain spectra associated with TE and TM modes of a waveguide and an MQW laser. In Section II, simplified models for polarization-dependent modal gains in bulk and MQW lasers are presented. In Section III, we report the results of numerical calculation, focusing on the nonuniformity dependence of optical modal gains of both polarizations. The ratio of TE-to-TM modal gain is also discussed, and we find that it is possible to detect the degree of nonuniformity of carrier distribution experimentally by measuring the TE/TM modal gain ratio.

II. Models

A. Bulk

We begin with a simplified model which distills the essential features of the physical system in question. We later consider the complex case of separate confined heterojunction (SCH) MQW lasers and semiconductor optical amplifiers (SOAs) in more detail.

We start by considering a three-layer slab waveguide in which an active region layer with the width of d is sandwiched between two cladding layers. The refractive indices are n_1 in the active layer and n_2 in the cladding layer. For symmetric TE and TM modes, the one-dimensional transverse electric (and magnetic) modal field profiles are given by [8]

$$E(H)_y = C_1 e^{ik_z z} \begin{cases} \cos\left(k_x \dfrac{d}{2}\right) e^{-\alpha(x-d/2)}, & x \geq d/2 \\ \cos(k_x x), & |x| \leq d/2 \\ \cos\left(k_x \dfrac{d}{2}\right) e^{\alpha(x+d/2)}, & x \leq -d/2 \end{cases} \tag{1}$$

where

$$C_1 = \frac{\left(\dfrac{4\omega\mu_1}{k_z d}\right)^{1/2}}{\left[1 + \dfrac{\sin k_x d}{k_x d} + \left(\dfrac{\mu_1}{\mu_2}\right)\left(\dfrac{2}{\alpha d}\right)\cos^2(k_x d/2)\right]^{1/2}} \quad \text{for TE modes} \tag{2a}$$

and

$$C_1 = \frac{\left(\dfrac{4\omega\varepsilon_1}{k_z d}\right)^{1/2}}{\left[1 + \dfrac{\sin k_x d}{k_x d} + \left(\dfrac{\varepsilon_1}{\varepsilon_2}\right)\left(\dfrac{2}{\alpha d}\right)\cos^2(k_x d/2)\right]^{1/2}} \quad \text{for TM modes.} \tag{2b}$$

The eigenvalue equation for the TE mode is

$$\alpha_{\mathrm{TE}} \frac{d}{2} = \frac{\mu_2}{\mu_1}\left(k_{x\_\mathrm{TE}} \frac{d}{2}\right) \tan\left(k_{x\_\mathrm{TE}} \frac{d}{2}\right) \tag{3}$$

and for the TM mode is

$$\alpha_{\mathrm{TM}} \frac{d}{2} = \frac{\varepsilon_2}{\varepsilon_1}\left(k_{x\_\mathrm{TM}} \frac{d}{2}\right) \tan\left(k_{x\_\mathrm{TM}} \frac{d}{2}\right). \tag{4}$$

α is given by

$$\alpha^2_{\mathrm{TE(TM)}} = \left(\frac{2\pi}{\lambda}\right)^2 (n_1^2 - n_2^2) - k^2_{x\_\mathrm{TE(TM)}}. \tag{5}$$

For simplicity, we approximate the carrier density profile in the active region using an ambipolar diffusion equation with an effective recombination time τ[1]

$$D \frac{d^2 n}{dx^2} = \frac{n}{\tau}. \tag{6}$$

For this equation to apply exactly, the ambipolar diffusion length must be a constant in space. This is evidently an approximation in the real physical scenario within a laser active region, but it does capture the possibility of a nonuniform distribution on carriers and gain. Solutions to this equation take the form of even and odd hyperbolic functions

$$n(x) = \gamma_{\mathrm{even}} \cosh(x/L) + \gamma_{\mathrm{odd}} \sinh(x/L) \tag{7}$$

in which L is the ambipolar diffusion length and is related to the ambipolar diffusivity and the effective recombination time according to $L^2 = D\tau$.

When carriers are well confined to the active region, as in a double-heterostructure laser, the carrier density profile may accurately be written [9]

$$n(x) = \frac{J_R \tau}{2eL}\left[\frac{\cosh(x/L)}{\sinh(d/2L)} - \frac{b-1}{b+1}\frac{\sinh(x/L)}{\cosh(d/2L)}\right] \tag{8}$$

where J_R is the recombination current density and b is the electron/hole mobility ratio μ_n/μ_p.

Modal gain is conventionally viewed as the product of confinement factor and bulk gain. In the presence of a nonuniform carrier distribution, and, therefore, a nonuniform gain distribution, it is necessary to return to a more fundamental definition [10]

$$\langle g \rangle_{\mathrm{TE}} = \frac{\displaystyle\int_{-d/2}^{d/2} g_{\mathrm{bulk}}(n) n_1 |E_y|^2 \, dx}{N_m \displaystyle\int_{-\infty}^{\infty} |E_y|^2 \, dx}$$

and

$$\langle g \rangle_{\mathrm{TM}} = \frac{N_m \displaystyle\int_{-d/2}^{d/2} g_{\mathrm{bulk}}(n) n_1 [|E_x|^2 + |E_z|^2] \, dx}{\displaystyle\int_{-d/2}^{d/2} n_1 |E_x|^2 \, dx + 2\int_{d/2}^{\infty} n_2 |E_x|^2 \, dx} \tag{9}$$

where $N_m = k_z/(2\pi/\lambda)$ is the mode index and $E_x = k_z/(\varepsilon\omega)H_y$ and $E_z = i/(\varepsilon\omega)(dH_y/dx)$ are the x- and z-directed electric fields of the TM mode. E_y is the only electric field component of the TE mode and H_y is the only magnetic field component of the TM mode. g_{TE} and g_{TM} represent the modal gains of TE and TM polarizations, each of which in turn

[1]Thus, we neglect in this subsection the exact configuration of the continuous carreier density profile in the simultaneous presence of Shockley–Read–Hall, spontaneous, Auger, and stimulated recombination. Instead, we focus on the approximate result which yields analytically direct results. The approximation is good for small to moderate nonuniformities.

depends on the local carrier density $n(x)$. For bulk material, good fitting results can be obtained to the functional form

$$g_{\text{bulk}}(n) = a(n - n_{\text{tr}}) \tag{10}$$

where a is the material gain coefficient and n_{tr} the transparency carrier density.

B. Multiple Quantum Wells

We employ a simplified version of the carrier injection and capture model of [5] in order to determine the distribution of carriers among a number of QWs. In our simplified model, the carrier density is treated as the sum of two populations: 3-D (unconfined, uncaptured) and 2-D (quantum confined, captured) carriers. Each population is distributed in space: 3-D carriers are described using continuity equations, and the 2-D population is treated separately in each well. The resulting set of equations is written

$$\frac{\partial}{\partial t} P_B(x, t) = \frac{\partial}{\partial x}\left(D\frac{\partial P_B(x, t)}{\partial x} - \mu P_B(x, t)E\right) - R_B - R_c = 0 \tag{11}$$

$$\frac{dP_{Qj}}{dt} = R_{cj} - R_{Qj} - G(P_{Qj})S \tag{12}$$

$$\frac{dS}{dt} = \sum_j [\Gamma_j G(P_{Qj})S + \Gamma_j \gamma B P_{Qj}^2] - \frac{S}{\tau_p} \tag{13}$$

$$J = q\left[-D\frac{\partial}{\partial x} P_B\left(-\frac{d}{2}, t\right) + \mu P_B\left(-\frac{d}{2}, t\right) E(-d/2, t)\right] = \frac{I}{A}. \tag{14}$$

Equation (11) is the continuity equation for the 3-D carriers, where D is the ambipolar diffusion coefficient, μ the ambipolar mobility. P_B is the 3-D carrier concentration, R_B the bulk recombination rate, R_c the net capture rate into the wells, and E is the electric field.

Equation (12) is the rate equation for the quantum-confined (subscript Q) carriers, in which P_{Qj} is the 2-D carrier density in the jth well. The net carrier capture rate into the jth well is R_{cj}. R_{Qj} is the recombination rate in the jth well, and $G(P_{Qj})$ is the gain at the lasing energy and is a function of the local carrier densities in the QW. It may generally be a function both of carrier density and photon density (due to gain compression). At low photon density, i.e., current injection in the vicinity of its threshold value, the photon density dependence of the gain may be neglected.

Equation (13) is the rate equation for the photon density S. The first term on the right-hand side of (13) is the sum of contributions of stimulated emission and spontaneous emission coupled to the lasing mode from the various wells. γ is the fraction of spontaneous emission coupled to the lasing mode, B is the bimolecular recombination coefficient, and τ_p is the photon lifetime.

Equation (14) is a definition of ambipolar current density which, at position $x = -d/2$, provides a boundary condition connecting injected current density with carrier density and electric field. For simplicity, we neglect the effect of leakage current, a mechanism which has been explored in detail elsewhere [11].

We solve a single carrier rate equation, in contrast with the coupled set of equations for electrons and holes used by Tessler and Eisenstein. Since the specific origin of carrier density nonuniformity is not the focus of this work, we use this approximation to simplify computation herein. The approximation is justified on physical and also quantitative grounds. Qualitatively, the carrier distribution is dominated by the lower-mobility carrier — heavy holes in pertinent compound semiconductors. Quantitatively, we have compared the calculated carrier density distribution among QWs using our simplified model with the results of Tessler and Eisenstein, finding good agreement in all cases considered in this work. The evolution of nonuniformity of carrier distribution with current injection observed in our simulation is also in agreement with Tessler and Eisenstein's work.

The recombination rates in bulk material and QWs are treated by taking account of the effects of Schockley–Read–Hall (SRH), spontaneous, and Auger recombination

$$R_B = AP_B(x, t) + BP_B^2(x, t) + CP_B^3(x, t) \tag{15}$$

$$R_{Qj} = AP_{Qj} + BP_{Qj}^2 + CP_{Qj}^3 \tag{16}$$

where A is the Shockley–Read–Hall recombination coefficient, B the bimolecular recombination coefficient, and C the Auger recombination coefficient.

We employ phenomenological capture and escape times as per the methods of other authors [12], so that the net carrier capture rate R_{cj} is given by

$$R_{cj} = \begin{cases} \dfrac{P_{Bj}}{\tau_c} - \dfrac{P_{Qj}}{\tau_e}, & x \in [x_0^j - W^j,\, x_1^j + W^j] \\ 0, & x \notin [x_0^j - W^j,\, x_1^j + W^j] \end{cases} \tag{17}$$

where τ_c and τ_e are, respectively, the carrier capture time from 3-D to 2-D and the carrier emission time from 2-D to 3-D.

In (17), the jth well is located between x_0^j and x_1^j and is of width W^j. The range $x_0^j - W^j$ to $x_1^j + W^j$ is defined as the capture range. P_{Bj} is the average 3-D carrier density in the capture range defined as

$$P_{Bj} = \frac{1}{3W^j}\int_{x_0^j - W^j}^{x_1^j + W^j} P_B(x)\, dx. \tag{18}$$

The gain in the jth well is related logarithmically to the carrier density according to [8]

$$G(P_{Qj}) = g_0\left(1 + \ln\left(\frac{P_{Qj}}{P_0}\right)\right) \tag{19}$$

where g_0 is the material gain coefficient and $P_0 e^{-1}$ is the transparency density. Our model takes account of polarization-dependent gain which arises due to the influence of strain on matrix elements and band structure. In our simulations, we account for the influence of strain through the use of different gain versus carrier dependencies for TE versus TM modes.

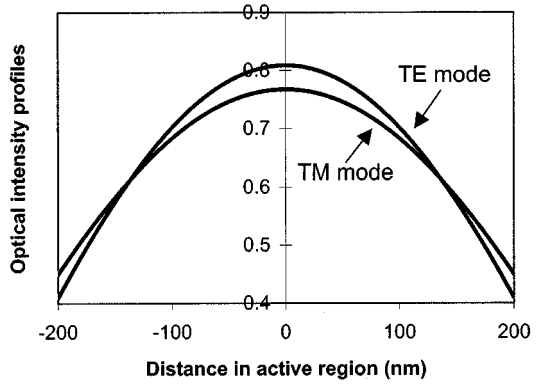

Fig. 1. Normalized TE and TM mode intensity profiles in the active region of the three-layer slab waveguide, assuming $\lambda = 1.55\ \mu$m, $n_1 = 3.6$, $n_2 = 3.0$, $\mu_1 = \mu_2 = 1$, $d = 0.4\ \mu$m.

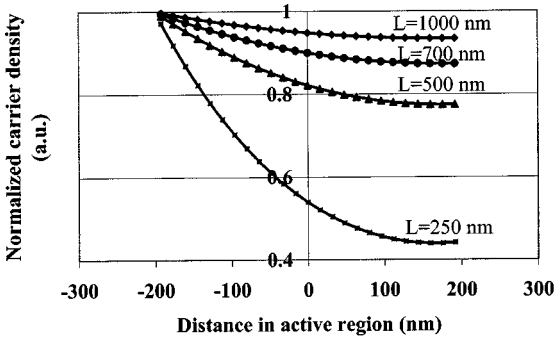

Fig. 2. Normalized carrier distribution profiles at different ambipolar diffusion lengths L. From top to bottom, $L = 1.0,\ 0.70,\ 0.5$, and $0.25\ \mu$m. The curves have been normalized so that the carrier density at the leftmost point is always unity.

The TE (TM) modal gain is entirely analogous to the bulk active region case:

$$\langle g\rangle_{\rm TE} = \frac{\displaystyle\sum_{j=1}^{N} n_1 g_{0\rm TE}\left(1+\ln\left(\frac{P_{Qj}}{P_0}\right)\right)|E_y(x_0^j)|^2 W^j}{N_m\displaystyle\int_{-\infty}^{\infty}|E_y|^2\,dx} \tag{20}$$

and as shown in (21), at the bottom of the page.

III. Effect of Nonuniformity of Carrier Distribution on Modal Gain

A. Bulk

In this section, we focus our consideration of bulk laser behavior on relating a generalized measure of the degree of carrier density nonuniformity (hence gain nonuniformity) with the polarization dependence of the modal gain. Our analysis is not limited in its applicability to single-mode devices; the methods and equations put forth herein make it possible to consider the interaction of a gain profile with an arbitrary mode profile. In order to provide a concrete and technologically relevant example, we let $\lambda = 1.55\ \mu$m, $n_1 = 3.6$, $n_2 = 3.0$, $\mu_1 = \mu_2 = 1.0$, and $d = 0.4\ \mu$m [13]. The normalized mode profiles associated with the TE and TM modes are shown in Fig. 1. The TE mode, which has a confinement factor $\Gamma_{\rm TE} = 0.90$, is more localized to the center of the active region than the TM mode, which has a confinement factor $\Gamma_{\rm TM} = 0.818$.

The electron/hole mobility ratio (b) is taken to be 15. Since electron mobility is much higher than hole mobility, the value of the hole diffusion length given by $(D\tau)^{1/2}$ provides a good estimate of ambipolar diffusion length. Carrier lifetimes can range from a few nanoseconds under low injection to ~70 ps in the presence of fast stimulated recombination due to high gain and photon density [14]. For hole mobilities in the range 50–75 $\rm cm^2V^{-1}s^{-1}$ in doped InGaAsP material [15], diffusivities will lie in the range $D = (KT/e)\times\mu = 1.3$–$1.95\ \rm cm^2s^{-1}$ and hole diffusion lengths, therefore, from ~100 to 500 nm. Thus, there will exist regimes of operation and device structures in which strong nonuniformities exist, and, under different circumstances and structural choices, there can exist a high degree of uniformity. In Fig. 2, we plot the carrier density distribution in the active region of the three-layer slab waveguide for four choices of ambipolar diffusion length L. In order to quantify the nonuniformity of carrier distribution, we define the normalized nonuniformity NU as

$$NU = \frac{\sqrt{\overline{n^2} - (\overline{n})^2}}{\overline{n}}. \tag{22}$$

The averaging of n or n^2 is performed over the spatial extent of the active region. We show in Appendix A that the normalized nonuniformity NU is approximately linear with d/L when d/L is less than 1.5:

$$NU \approx \frac{1}{2\sqrt{3}}\,\frac{d}{L}. \tag{23}$$

To illustrate the influence of the carrier nonuniformity on TE and TM modal gains, we plot in Fig. 3 the TE and TM modal gains as a function of NU by fixing the recombination current density J_R and the active layer thickness d and varying the diffusion length L. It is apparent from Fig. 3 that TE and TM gains are influenced differently by the changing degree of carrier density nonuniformity. In order to bring out any such relative changes,

$$\langle g\rangle_{\rm TM} = \frac{\displaystyle\sum_{j=1}^{N} N_m n_1 g_{0\rm TM}\left(1+\ln\left(\frac{P_{Qj}}{P_0}\right)\right)\left[|E_x(x_0^j)|^2 + |E_z(x_0^j)|^2\right] W^j}{\displaystyle\int_{-d/2}^{d/2} n_1^2|E_x|^2\,dx + 2\int_{d/2}^{\infty} n_2^2|E_x|^2\,dx} \tag{21}$$

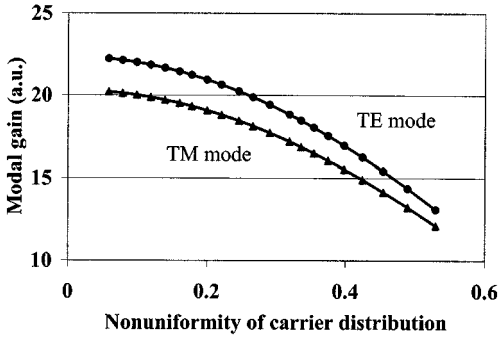

Fig. 3. TE and TM modal gains as functions of the nonuniformity of carrier distribution. Active layer thickness $d = 400$ nm, $a_{\rm TE} = a_{\rm TM} = 3.0 \times 10^{-22}$ m^{-2}, $\tau = 9 \times 10^{-9}$ s, $n_{tr} = 1.0 \times 10^{24}$ m^{-3} [16], and $J_R = 7.7 \times 10^6$ A/m^2.

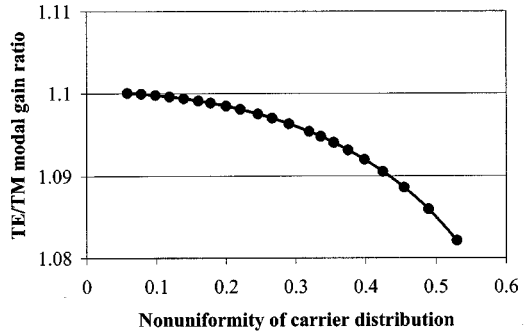

Fig. 4. The ratio of TE and TM modal gains as a function of the nonuniformity of carrier distribution. Active layer thickness $d = 400$ nm, $a_{\rm TE} = a_{\rm TM} = 3.0 \times 10^{-22}$ m^{-2}, $n_{\rm tr} = 1.0 \times 10^{24}$ m^{-3} [16], and $J_R = 7.7 \times 10^6$ A/m^2.

we plot in Fig. 4 the ratio of TE to TM modal gain as a function of NU.

In order to ensure a fair comparison, we fixed the recombination current density but changed the ambipolar diffusion length in our simulations so that the carrier nonuniformity is intentionally modified while the average carrier density in the active region remains constant. The relative evolution of TE versus TM modal gains apparent from Figs. 3 and 4 comes from the changing shape of the gain distribution relative to the mode profile. The broader TM mode samples the outer reaches of the active region; the TE mode is more localized to the center of the active region and, as such, samples the portion of the active region which becomes more depleted of carriers as the carrier nonuniformity increases. As a consequence, the TE modal gain is degraded relatively more than the TM modal gain as the carrier distribution in the active region becomes more nonuniform. The ratio of TE-to-TM modal gain in the presence of a uniform gain distribution is equal to conventionally defined TE to TM confinement factor ratio ($\Gamma_{\rm TE}/\Gamma_{\rm TM} = 1.1$) since the gain distribution can, under this scenario, be taken out from the integral of (9). The deviation of this ratio increases with growing carrier density nonuniformity. The experimentally measurable quantity (TE/TM modal gain ratio) therefore contains information about the degree of carrier density nonuniformity. Our results for the bulk case are illustrative, in the conceptually simpler bulk (continuous carrier density distribution) case, of the physical phenomenon presented throughout this work. We find later in this work that the quantitative influence of nonuniformity effects are much greater in the more mathematically and conceptually complex case of an MQW active region.

We have focused our attention on the impact of gain nonuniformity along a single specific 1-D axis. Nonuniformity can potentially exist along both transverse dimensions. In the lateral direction, it may result from hole burning connected with spatially varying stimulated emission whose rate is proportional to the local photon density. In the vertical (thinner) direction, it is most strongly linked with the injection of carriers of dramatically differing mobilities from opposite sides of the active region. If desired, the effects of these mechanisms acting along orthogonal axes could readily be included simultaneously: in the effective index approximation, this would be proportional to a product of influences along the two basis directions. In the presence of a known mode shape and a known gain profile, we may obtain the resulting TE/TM modal gain ratio, as illustrated above. In reality, the mode shape may be influenced by a combination of gain-guiding and free-carrier plasma-induced refractive index change. Thus, the mode shape and gain profile influence one another mutually. The parametric relationships derived in this work make it possible to take self-consistent account of these combined effects in order to obtain the comprehensive above-threshold laser characteristic.

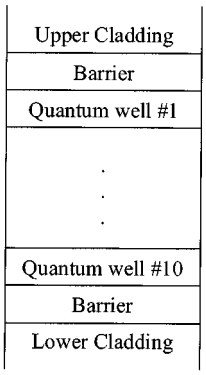

Fig. 5. Schematic diagram of a 10-QW structure used in the simulations. The total width of the active region is 0.4 μ. The starting and ending positions of the jth well are $x_0^j = (-0.208 + 0.04j)$ μm and $x_1^j = (-0.2 + 0.04j)$ μm. The width of a single QW is $W^j = 8$ nm.

B. Multiple Quantum Wells

We consider for illustrative purposes an MQW structure (Fig. 5) which consists of ten QWs and eleven barrier layers. The total active region thickness, effective index, and outer cladding layer refractive indices are the same as for the bulk active region case considered in the preceding section.

Calculated and experimental Auger coefficients for InGaAsP–InP MQWs intended for 1.55-μm operation have been found to depend on the details of the active region structure [17], varying between 10^{-28} and 10^{-27} cm^6·s^{-1}. For quantitative calculations in the present work, we employ the recombination rate parameters obtained by Chuang *et al.* [18] and given in Table I. The distribution of carrier density among the QWs is calculated employing (11)–(19) with physical quantities given in [5] and [19]–[22] and also listed in Table I.

TABLE I
MATERIAL PARAMETERS USED IN MQW CALCULATIONS

Ambipolar diffusion coefficient	$D = 0.0005\ m^2/s$
Ambipolar mobility	μ=0.01 m^2/Vs
Capture time*	τ_c=1×10^{-12} s
Escape time*	τ_e=3×10^{-11} s
Photon lifetime*	τ_p=2.1×10^{-12} s
SRH coefficient	$A = 1.1\times10^8\ s^{-1}$
Bimolecular coefficient	$B = 1\times10^{-16}\ m^3/s$
Auger coefficient	$C = 1.1\times10^{-39}\ m^6/s$
Spontaneous-emission factor	$\gamma = 5\times10^{-5}$

*See Appendix II.

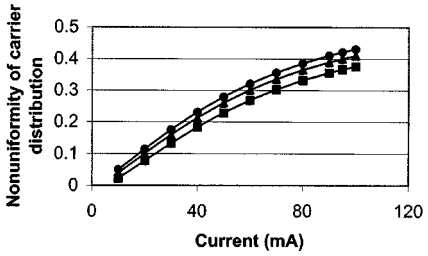

Fig. 6. Nonuniformity of carrier distribution in the ten quantum wells structure as a function of current injection. Solid dot: using carrier lifetime which is around 200 ps; Solid square: using carrier lifetime of around 750 ps; Solid triangle: using intermediate carrier lifetime;.

Using the numerical values given above, we calculate the carrier distribution profile under different injected currents. We obtain a strongly nonuniform distribution of carrier among QWs (shown in Fig. 6), with the most extreme pile-up of carriers occurring on the p-cladding side of the active region from which the less mobile type of carrier is injected.

In a semiconductor amplifier, another significant nonuniformity in the carrier distribution will be observed along the longitudinal extent of the amplifier cavity. This effect may exist in semiconductor lasers—particularly those with strongly asymmetric facet reflectivities [23]—but is particularly apparent in amplifiers in which photons experience a single pass of the cavity in view of the very low facet reflectivities employed. At the input facet, the photon density and stimulated recombination rate are low. The carrier lifetime is thus a maximum at the input facet, and the carrier density distribution the most uniform. The opposite situation arises at the output facet, at which the photon density is high, the stimulated recombination rate a maximum, the effective carrier lifetime is short, and the carrier distribution maximally nonuniform. The carrier lifetime in a typical semiconductor amplifier has been measured to be in a range between 200–750 ps [24]. We plot in Fig. 6 the carrier nonuniformity as a function of current injection for this range of carrier lifetimes. The resulting impact on the full device is bounded by these extreme cases.

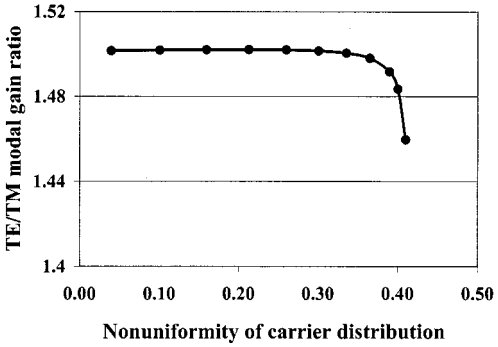

Fig. 7. TE/TM modal gain ratio as a function of nonuniformity of carrier distribution in the MQW structure

QW gain is anisotropic, with the TM-mode gain arising from conduction-band to light-hole transitions, and the TE-mode gain arising mostly from heavy-hole transitions. In agreement with [25], we take the ratio of TE to TM material gain coefficient in (19) to be $(\Gamma_{QW\_TM} g_0^{\mathrm{TE}})/(\Gamma_{QW\_TE} g_0^{\mathrm{TM}}) = 150/100$.

We show in Fig. 7 the calculated ratio of TE to TM modal gain as a function of carrier nonuniformity. We vary the injected current density while keeping the average carrier density among the wells constant. As in the bulk active region case, the ratio of TE to TM modal gain decreases with increasing carrier density nonuniformity among the wells. The TE modal gain is more degraded than the TM modal gain when the carrier density nonuniformity is increased, as in the bulk case depicted in Fig. 4. Comparing to the bulk active region case, the change of TE to TM modal gain ratio at higher carrier distribution nonuniformity is more significant in the QW case. This can be attributed to the different behavior of the linear (in the bulk case) and the logarithmic (in the QW) gain versus carrier density functions.

We have thus found a typical change in TE/TM modal gain of the order of 1% as carrier density nonuniformity evolves. It has previously been found experimentally that gain can be measured to within better than 0.14% [26]. While a single polarization will usually dominate the lasing spectrum above threshold, careful measurement permits simultaneous monitoring of the evolution of modal gain of both lasing and nonlasing TE and TM modes after the onset of lasing. This has been reported experimentally in both bulk [27] and QW [25] lasers. The facet reflectivity of a semiconductor amplifier is much lower than that of a cleaved semiconductor laser, and the photon lifetime in the cavity much reduced, as discussed in Appendix B. We obtain results similar to those shown in Fig. 7 using a low photon lifetime of a typical semiconductor optical amplifier.

The nature of the spatial relationship between photon and gain profiles can either aggravate or attenuate the injection level dependence of the TE/TM modal gain ratio. We consider in Fig. 8 the impact of displacing the position of the peak of the optical mode from the vertical center of the waveguide toward one of the cladding layers. Such an offset may be significant particularly in ridge waveguide devices in which the waveguide mode senses the nonequivalence of the upward and downward

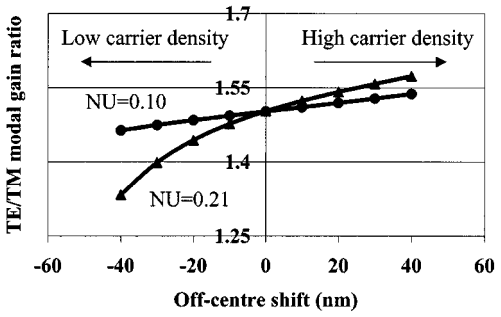

Fig. 8. TE/TM modal gain ratio as a function of off-center shift under different degrees of carrier distribution nonuniformity, $NU = 0.1$ and 0.21. Off-center shift is the offset of the optical mode peak of both polarizations from the center of the waveguide. For negative (positive) shift, the optical mode peak is pushed into the side with low (high) carrier density, corresponding to the contact from which electrons (holes) are injected.

directions. As seen in Fig. 8, when both modes are pushed in the direction of the higher carrier density (p-injector, positive offset) side of the active region, the injection level dependence of the modal gain ratio is decreased. When the mode is offset toward the higher gain QWs, most of the modal gain occurs near the (symmetric) centers of the modes, and the sensitivity of the polarization dependence to changing nonuniformity is reduced. On the other hand, if the mode is offset toward the lower carrier density (n-injector, negative offset) side of the active region, more of the modal gain comes from sampling the tails of the mode profiles. Since it is in the tails that the mode profiles differ most, the injection level dependence of the modal gain ratio is amplified.

These results are of use in designing SOAs in which polarization-independent operation is desired and must be preserved in the face of either changing bias levels or dynamic responses to time-dependent inputs. If the waveguide and active region are designed for polarization independence at a given bias level, this effect will best be maintained over a range of levels of operation if the waveguide is designed such that both TE and TM modes are offset from the vertical center of the waveguide in the direction of the hole-injecting contact.

IV. Conclusion

We have investigated TE and TM modal gains under carrier distribution profiles with varying degrees of nonuniformity. A nonuniform carrier distribution in either a bulk or an MQW active region degrades the modal gain seen by each polarization. There exist differences in the dependence of TE versus TM modal gain on carrier density nonuniformity. We have shown that this effect is attributable to the differences in the spatial mode profiles associated with the two orthogonal polarizations. Our results find application in the following areas.

1) Obtaining maximally direct measures of the evolution of internal carrier density distributions in semiconductor quantum optoelectronic devices. To date, these effects have been studied directly only via modeling, with their importance in real experimental observation of performance degradation being the subject of speculation rather than definitive demonstration.
2) Reducing injection level dependence of polarization insensitivity in MQW SOAs.
3) Increasing, as desired, polarization sensitivity and polarization variability in polarization-bistable functional optoelectronic devices [28].

Appendix A

Derivation of relation of NU and diffusion length L in bulk active region.

NU is defined in (22), where

$$\overline{n^2} = \frac{1}{d}\int_{-d/2}^{d/2} (n(x))^2\,dx$$

and

$$\overline{n} = \frac{1}{d}\int_{-d/2}^{d/2} n(x)\,dx. \tag{A1}$$

We substitute only the first term in (8) into the integration, which would be much simpler but does not affect the correctness of our conclusion

$$n(x) = \frac{J_R\tau}{2eL}\left[\frac{\cosh(x/L)}{\sinh(d/2L)}\right] \tag{A2}$$

and we obtain (A3), shown at the bottom of the page, where $x = d/L$.

Using the approximation of $e^x = 1 + x + x^2/2 + x^3/6 + x^4/24$, (A3) would be simplified to

$$\text{NU} \approx \frac{1}{2\sqrt{3}}\,x. \tag{A4}$$

The approximation is valid if $x < 1.5$.

Appendix B

The electron capture time is typically $\tau_c \approx 1$ ps, and the ratio of τ_e versus τ_c is structure- and bias-dependent [5]. The ratio increases with barrier height and decreases once the carrier density exceeds 10^{24} m^{-3} at which point QW charging effects become significant. For simplification of the calculations in this paper, τ_e and τ_c are fixed to be 3×10^{-10} s and 1×10^{-12} s, respectively. The photon lifetime τ_p is given by

$$\frac{1}{\tau_p} = \frac{c}{n_1}\left(\alpha_i + \frac{1}{2l}\ln\left(\frac{1}{R_1R_2}\right)\right). \tag{A5}$$

$$\text{N.U.} = \frac{\sqrt{(e^{2x}+e^{-2x}) + 4x(e^x - e^{-x}) + 4x^2 - 16(e^x+e^{-x}) + 30}}{4(e^{x/2} - e^{-x/2})} \tag{A3}$$

Given the intrinsic optical loss $\alpha_I = 3000\ \mathrm{m}^{-1}$, the cavity length $l = 400\ \mu$m, the group index $n_1 = 3.6$, and facet power reflectivity of a cleaved semiconductor laser R_1 and $R_2 = 0.32$, $\tau_p = 2.1 \times 10^{-12}$ s.

For a semiconductor amplifier, the facet power reflectivity is much lower than that for a laser. The typical value of the facet reflectivity (R_1 and R_2) is around 0.01% [24], yielding $\tau_p = 0.46 \times 10^{-12}$ s.

REFERENCES

[1] B. L. Lee, C. F. Lin, J. W. Lai, and W. Lin, "Experimental evidence of nonuniform carrier distribution in multiple-quantum-well laser diodes," *Electron. Lett.*, vol. 34, pp. 1230–1231, 1998.

[2] R. Nagarajan, M. Ishikawa, T. Fukushima, R. S. Geels, and J. E. Bowers, "High speed quantum-well lasers and carrier transport effects," *IEEE J. Quantum Electron.*, vol. 28, pp. 1990–2008, 1992.

[3] J. Piprek, P. Abraham, and J. E. Bowers, "Effects of quantum well recombination losses on the internal differential efficiency of multi-quantum-well lasers," in *IEEE 16th Int. Semiconductor Laser Conf.*, 1998, pp. 167–168.

[4] P. Landais, G. H. Duan, S. Keller, and J. Jacquet, "Nonuniform injection current induced unusual chirp behavior of a four electrode bistable distributed Bragg reflector laser," *IEEE J. Quantum Electron.*, vol. 31, pp. 1029–1037, 1995.

[5] N. Tessler and G. Eisenstein, "On carrier injection and gain dynamics in quantum well lasers," *IEEE J. Quantum Electron.*, vol. 29, pp. 1586–1595, 1993.

[6] A. Champagne, R. Maciejko, and T. Makino, "Enhanced carrier injection efficiency from lateral current injection in multiple-quantum-well DFB lasers," *IEEE Photon. Technol. Lett.*, vol. 8, pp. 749–751, 1996.

[7] H. Li, X. Q. Wang, and S. D. Hersee, "The measurement of lateral index variations in unstable resonator semiconductor lasers from spectrally resolved near-field images," *IEEE Photon. Technol. Lett.*, vol. 9, pp. 31–33, 1997.

[8] S. L. Chuang, *Physics of Optoelectronic Devices*. New York, NY: Wiley, 1995.

[9] A. Herlet, "Forward characteristic of silicon power rectifiers," *Solid State Electron.*, vol. 11, pp. 723–742, 1968.

[10] Y. Z. Huang, Z. Pan, and R. H. Wu, "Analysis of the optical confinement factor in semiconductor lasers," *J. Appl. Phys.*, vol. 79, pp. 3827–3830, 1996.

[11] I. M. P. Aarts and E. H. Sargent, "Above-threshold leakage in semiconductor lasers: An analytical physical model," *IEEE J. Quantum Electron.*, vol. 36, pp. 496–501, Apr. 2000.

[12] C. Y. Tsai, C. Y. Tsai, Y. H. Lo, R. M. Spencer, and L. F. Eastman, "Nonlinear gain coefficients in semiconductor quantum-well lasers: Effects of carrier diffusion, capture, and escape," *IEEE J. Select. Topics Quantum Electron.*, vol. 1, pp. 316–330, 1995.

[13] B. Mersali, G. Gelly, A. Accard, J. L. Lafragette, P. Doussiere, M. Lambert, and B. Fernier, "1.55 μm high-gain polarization-insensitive semiconductor travelling wave amplifier with low driving current," *Electron. Lett.*, vol. 26, pp. 124–125, 1990.

[14] M. Usami, M. tsurusawa, and Y. Matsushima, "Mechanism for reducing recovery time of optical nonlinearity in semiconductor laser amplifier," *Appl. Phys. Lett.*, vol. 72, pp. 2657–2659, 1998.

[15] J. R. Hayes, A. R. Adams, and P. D. Greene, *GaInAsP Alloy Semiconductors*, T. P. Pearsall, Ed. New York, NY: Wiley, 1982, ch. 8.

[16] N. K. Dutta, "Calculated absorption, emission, and gain in $In_{0.72}Ga_{0.28}As_{0.6}P_{0.4}$," *J. Appl. Phys.*, vol. 51, pp. 6095–6100, 1980.

[17] J. Wang, P. von Allmen, J. P. Leburton, and K. J. Linden, "Auger recombination in long-wavelength strained-layer quantum-well structures," *IEEE J. Quantum Electron.*, vol. 31, pp. 864–875, 1995.

[18] J. Minch, S. H. Park, T. Keating, and S. L. Chuang, "Theory and experiment of $In_{1-x}Ga_xAs_yP_{1-y}$ and $In_{1-x-y}Ga_xAl_yAs$ long-wavelength strained quantum-well lasers," *IEEE J. Quantum Electron.*, vol. 35, pp. 771–782, 1999.

[19] J. R. Hayes, A. R. Adams, and P. D. Greene, "Mobility of holes in the quaternary alloy InGaAsP," *Electron. Lett.*, vol. 16, pp. 282–284, 1980.

[20] P. D. Greene, S. A. Wheeler, A. R. Adams, A. N. El-Sabbahy, and C. N. Ahmad, "Background carrier concentration and electron mobility in LPE InGaAsP layers," *Appl. Phys. Lett.*, vol. 35, pp. 78–80, 1979.

[21] D. X. Zhu, S. Dubovitsky, W. H. Steier, J. Burger, D. Tishinin, K. Uppal, and P. D. Dapkus, "Ambipolar diffusion coefficient and carrier lifetime in a compressively strained InGaAsP multiple quantum well device," *Appl. Phys. Lett.*, vol. 71, pp. 647–649, 1997.

[22] G. P. Agrawal and N. K. Dutta, *Semiconductor Lasers*. New York, NY: Van Nostrand Reinhold, 1993.

[23] E. H. Sargent, D. Pavlidis, H. Anis, N. Golinescu, J. M. Xu, R. Clayton, and H. B. Kim, "Longitudinal carrier density profiling in semiconductor lasers via spectral analysis of side spontaneous emission," *J. Appl. Phys.*, vol. 80, pp. 1904–1906, 1996.

[24] N. Storkfelt, B. Mikkelsen, D. S. Olesen, M. Yamaguchi, and K. E. Stubkjaer, "Measurement of carrier lifetime and linewidth enhancement factor for 1.5-μm ridge-waveguide laser amplifier," *IEEE Photon. Technol. Lett.*, vol. 3, pp. 632–634, 1991.

[25] D. P. Bour, K. J. Beernink, D. W. Treat, T. L. Paoli, and R. L. Thornton, "Dual-polarization, single quantum-well AlGaInP laser diode structure," *IEEE J. Quantum Electron.*, vol. 30, pp. 2738–2742, 1994.

[26] D. T. Cassidy, "Technique for measurement of the gain spectra of semiconductor diode lasers," *J. Appl. Phys.*, vol. 56, pp. 3096–3099, 1984.

[27] B. W. Hakki and T. L. Paoli, "Gain spectra in GaAs double-heterostructure injection lasers," *J. Appl. Phys.*, vol. 46, pp. 1299–1306, 1975.

[28] J. M. Liu and V. C. Chen, "Digital optical signal processing with polarization-bistable semiconductor lasers," *IEEE J. Quantum Electron.*, vol. QE-21, pp. 298–306, 1985.

Dayan Ban, photograph and biography not available at the time of publication.

Edward H. Sargent (S'97–M'98) holds the Nortel Junior Chair in Emerging Technologies in the Department of Electrical and Computer Engineering at the University of Toronto, Toronto, ON, Canada. He leads a group of 12 graduate and post-doctoral researchers in the areas of semiconductor quantum electronic devices, photonic crystal applications, hybrid organic–inorganic quantum dot electroluminescence, and multiple-access optical networks.

Prof. Sargent was awarded the Silver Medal of the Natural Sciences and Engineering Research Council of Canada in 1999 for his work on lateral current injection lasers. Also, in 1999, he won the Premier's Research Excellence Award in recognition of research into the application of photonic crystals in lightwave systems.